Identification of *PDE4D* as a proliferation promoting factor in prostate cancer using a *Sleeping Beauty* transposon based somatic mutagenesis screen

Eric P. Rahrmann[*,1], **Lara S. Collier**[*,2], **Todd P. Knutson**[1], **Meghan E. Doyal**[1], **Sheri L. Kuslak**[1], **Laura E. Green**[1], **Rita L. Malinowski**[2], **Laura Roethe**[2], **Keiko Akagi**[3], **Michelle Waknitz**[4], **Wei Huang**[4], **David A. Largaespada**[1], and **Paul C. Marker**[2]

[1]Department of Genetics, Cell Biology, and Development and Masonic Cancer Center, University of Minnesota, Minneapolis, Minnesota, 55455, USA

[2]Division of Pharmaceutical Sciences, School of Pharmacy and UW Carbone Comprehensive Cancer Center, University of Wisconsin-Madison, Madison, Wisconsin, 53705, USA

[3]Mouse Cancer Genetics Program, National Cancer Institute in Frederick, Frederick, MD, 21702, USA

[4]Department of Pathology and Laboratory Medicine, University of Wisconsin-Madison, Madison, Wisconsin, 53705, USA

Abstract

Retroviral and transposon-based mutagenesis screens in mice have been useful for identifying candidate cancer genes for some tumor types. However, many of the organs that exhibit the highest cancer rates in humans, including the prostate, have not previously been amenable to these approaches. This study demonstrates for the first time that the *Sleeping Beauty* transposon system can be used to identify candidate prostate cancer genes in mice. Somatic mobilization of a mutagenic transposon resulted in focal epithelial proliferation and hyperplasia in the prostate. Efficient methods were established to identify transposon insertion sites in these lesions, and analysis of transposon insertions identified candidate prostate cancer genes at common insertion sites, including *Pde4d*. *PDE4D* was also over-expressed in human prostate cancer patient samples and cell lines, and changes in *PDE4D* mRNA isoform expression were observed in human prostate cancers. Furthermore, knockdown of *PDE4D* reduced the growth and migration of prostate cancer cells *in vitro*, and knockdown of *PDE4D* reduced the growth and proliferation rate of prostate cancer xenografts *in vivo*. These data indicate that *PDE4D* functions as a proliferation promoting factor in prostate cancer, and the *Sleeping Beauty* transposon system is a useful tool for identifying candidate prostate cancer genes.

INTRODUCTION

Forward somatic mutagenesis screens using murine retroviruses as insertional mutagens have been effective tools for cancer gene discovery in mammary tumors, hematopoietic neoplasms, and brain tumors in mice (1–3). However, many tissue types that are commonly transformed into tumors in humans are not affected by known retroviruses. Two studies have shown that genome-wide somatic mutagenesis using the *Sleeping Beauty* (SB) transposon system can be

Corresponding Author: Paul C. Marker, Division of Pharmaceutical Sciences, School of Pharmacy, University of Wisconsin, Madison, 777 Highland Ave., Madison, WI 53705 (608)890-2150 (voice), (608)262-5345 (FAX), E-mail: marker@wisc.edu.
*equal contribution

used to induce tumors and identify cancer genes for hematopoietic tumors and sarcomas (4, 5). Candidate cancer genes were identified in these studies by finding sites in the genome of SB-induced tumors that were recurrently mutated by transposon insertions in multiple independent tumors. Such sites are called common insertion sites (CISs), and past experience with retroviral-based and transposon-based screens has shown that the genes located at CISs act as oncogenes or tumor suppressors. A major unresolved question for this approach is whether or not SB will be more broadly applicable for cancer gene discovery in epithelial cancers which are responsible for 80% of human cancer deaths (6).

Prostate adenocarcinoma is the most commonly diagnosed male cancer and is one of the leading causes of male cancer death (6). Prior to the development of invasive adenocarcinoma, several histologic abnormalities can sometimes be observed that are considered potential precursor lesions for prostatic adenocarcinoma. These include prostatic intraepithelial neoplasia (PIN), atypical small acinar proliferation (ASAP), and proliferative inflammatory atrophy (PIA) (7, 8). Features associated with one or more of these candidate precursor lesions include focal areas of increased proliferation, stratification of the epithelium, loss of basal cells, and changes in nuclear morphology. Several genetic and gene expression alterations have been identified as common events in early prostate cancers. The transcription factor *Nkx3.1* is commonly lost in early stage tumor epithelial cells, including loss in 20% of high grade PIN cases examined (9). This loss of expression is likely due to heterozygous deletions of the genomic locus and epigenetic silencing mechanisms (10). Recurrent deletions and translocations that create fusion genes involving transcription factors ERG, ETV1, or ETV4 in prostate epithelial cells have been reported to occur in a majority of prostate cancers, and are also detected as early as PIN (11–13). Although these genetic alterations clearly play a role in early prostate cancers, the genetic basis for prostate cancer initiation remains poorly understood (14). In this study, transposon-based somatic mutagenesis caused foci of altered histology and elevated proliferation in the prostatic epithelium that resembled features associated with prostate cancer precursor lesions. Analysis of transposon insertion sites in these lesions identified candidate cancer genes that may play a role in prostate cancer initiation, including *PDE4D*. PDE4D was also over-expressed in human prostatic adencarcinomas, and shRNA knockdown of PDE4D reduced the proliferation of prostate cancer cells *in vitro* and *in vivo*, supporting its potential role as a proliferation promoting factor in human prostate cancer.

MATERIALS AND METHODS

Mice

The mouse strains utilized for this study have previously been described including CAGGS-SB10 transgenic, *Rosa26*-SB11 knock-in, and low-copy T2/onc transgenic (4,5).

Immunohistochemistry

Tissues were stained for the Ki67 antigen as previously described (15). A modified staining protocol was used for laser capture microscopy as follows: tissues were dissected into cold PBS, embedded directly into Tissue Freezing Medium (Triangle Biomedical Sciences) and stored at −80°C. Tissue sections (5µm) were cut at −20°C with a cryostat and immediately mounted onto PEN membrane slides (Leica) and air-dried for 30 minutes followed by fixation in 100% ethanol at −20°C. Slides were washed with PBS, blocked with 2.5% sheep serum in PBS, stained for 3 hours with anti-phospho-Histone-H3 (Upstate Cell Signaling Solutions) 1:150 in 2.5% sheep serum in PBS, and washed in PBT (PBT = 1X PBS with 0.1% Tween 20). The primary antibody was visualized with an anti-rabbit IgG horseradish peroxidase conjugate (Chemicon) diluted 1:500 in 2.5% sheep serum in PBS followed by PBT washes and staining with the DAB reagent (Vector Laboratories) according to the manufacturer's

instructions. Slides were counter stained with Hematoxylin, dehydrated into 100% ethanol, and air dried for 1 hour prior to laser capture.

Laser capture microscopy and Liner-mediated PCR

Cells of interest were captured from tissue sections using a Leica LMD6000 laser capture microdisection microscope. DNA was isolated from the captured cells using a Qiagen Qiamp DNA Micro Kit according to the manufacturer's instructions except GenomiPhi DNA amplification sample buffer was substituted for the Qiagen elution buffer during the last step of DNA purification. Samples were then amplified using the GenomiPhi DNA Amplification Kit (GE Healthcare) according to the manufacturer's instructions. Transposon-genomic DNA junctions were amplified as previously described (16), cloned into plasmids, and sequenced by Functional Biosciences Inc.

AQUA Analysis of PDE4D expression

The AQUA analysis was conducted on a previously assembled tissue microarray (TMA) of prostate tissues from patients treated at the University of Wisconsin-Madison using an established protocol (17). Epithelial compartment visualization was achieved with a 30 minute incubation of a mouse anti-cytokeratin AE1/AE3 1:200 (Dako North America, Carpinteria, CA) and mouse anti-E-cadherin 1:50 (Abcam, Cambridge, MA) cocktail, followed by a 30 minute incubation of Invitrogen Alexa Fluor 555 donkey anti-mouse IgG 1:200. Goat anti-PDE4D IgG 1:100 (Santa Cruz, Santa Cruz, CA) was preincubated with PDE4D protein (5x wt:wt) (Santa Cruz, Santa Cruz, CA) for 2 hr 30 min. prior to application. Both PDE4D antibody 1:100 and PDE4D with 5x protein were incubated for 60 minutes followed by a 15 minute incubation with Invitrogen biotinylated swine anti-goat IgG 1:200. Staining on the TMA was visualized as previously described (17). There were 336 tissue cores from 168 patients (2 cores from each patient) in the TMA stained for this study. In addition to an automated image acquisition and analysis as previously described (18), all cores for this study were examined for staining and morphology by surgical pathologist, Wei Huang, MD. TMA cores without sufficient epithelium (<5%) or with poor staining quality (i.e., section folding, excess trapping of fluorochrome, etc.) were excluded from analysis. In total, 282 of the 336 cores stained for PDE4D passed this quality control and were included in the final data set.

RLM-5'-RACE

The RNA analyzed in the RLM-5'-RACE experiment was isolated from human prostate samples obtained by the University of Minnesota Cancer Center Tissue Procurement Facility (TPF). For the study, prostate tissue samples were bisected. One piece was provided to our laboratory as a fresh sample that was used for the isolation of RNA. The adjacent piece of tissue was retained by the TPF for examination by a TPF staff pathologist who provided us with a pathology report that indicated the presence/absence and pathological grade of prostate cancer in each tissue sample. RNAs were analyzed using the FirstChoice RLM-RACE kit (Ambion) according to the manufacturer's instructions. The PDE4D outer and inner primers were 5-TAGGCCACATCAGCATGGTAATGGTCT-3' and 5'-ACCACTAGTTCACATCTTCTAGTTCCTTGGCAAGGA respectively.

Cell Culture

DU145-derived cell lines were grown in 1xRPMI (Invitrogen Gibco) supplemented with 5% activated charcoal USP (Sigma) treated fetal bovine serum (Hyclone), 100µg/ml antibiotic/antimycotic (Invitrogen Gibco), and 10^{-8}M 5α-androsten-17β-ol-3-one (Sigma). PC3-derived cell lines were grown in 1xMEM (Invitrogen Gibco) supplemented with 5% activeated charcoal USP (Sigma) treated fetal bovine serum (Hyclone), 100µg/ml antibiotic/antimycotic (Invitrogen Gibco), 1xNon-essential amino acids (Invitrogen Gibco), and 1xSodium Pyruvate

(Invitrogen Gibco). All cell lines were grown at 37°C in 5% CO_2. Stable *PDE4D* shRNA knockdown and scrambled sequence shRNA control cell lines were generated using lentiviral transduction with shRNAs from Open Biosystems. Cells were transduced at a multiplicity of infection of 10 following manufacturers protocol and then underwent G418 selection for stable integrants. Immunoblots of cell line extracts were conducted as previously described (15) using the anti-PDE4D antibody (Abcam) diluted 1:1500 in 2.5% milk.

Growth Assays

Cells were plated at an initial density of 5,000 cells/cm^2 on 4-well plates (Costar). After the growth period, cells were trypsinized, neutralized in media, and trypan blue was added. The number of viable cells was determined by counting the number of cells that exclude trypan blue on a hemacytometer. Alternatively, cells were plated at an initial density of 500 cells per well on a 96 well plate in triplicate, and cell viability was evaluated using an MTS assay (the CellTiter96 Aqueous One Solution Cell Proliferation Assay from Promega) according to the manufacturer's instructions.

Xenograft assay

Cultured cells were trypsinized, resuspended at 10^6 cells in 500µl of Matrigel (BD Biosciences 356230), and injected subcutaneously into CD-1 nu/nu mice. After 1 month, xenografts were fixed in formalin and processed for IHC. Following Ki67 staining, 8 random 20X fields were photographed and the ratio of Ki67 positive nuclei to total nuclei was determined using a previously described computer-assisted method for image analysis (19).

RESULTS

Focal hyperplasia in the prostatic epithelium of transposon mutagenized mice

Previous studies showed that two mouse strains with active transposition of a mutagenic transposon, T2/onc, became moribund due to the formation of tumors with a limited tissue distribution (4,5). The two strains used in these experiments differed in the transgene driving transposase expression (CAGGS-SB10 or *Rosa26*-SB11). In addition, the CAGGS-SB10;T2/onc mice were null for the *Arf* tumor suppressor gene. We examined the morphology and histology of prostate glands from CAGGS-SB10;T2/onc low-copy;*Arf*-/- mice, and the only prostatic abnormalities identified were infrequent sarcomas (data not shown). We also evaluated *Rosa26*-SB11;T2/onc low-copy (approximately 25 copies of T2/onc) mice. Unlike the previously reported high rate of embryonic lethality in *Rosa26*-SB11;T2/onc high-copy (148+ copies of T2/onc) mice (4), the ratio of *Rosa26*-SB11;T2/onc low-copy mice to single transgenic littermates was consistent with little or no embryonic lethality. However, these mice succumbed to tumor formation, primarily leukemias, with an median latency of 6–7 months (Lara Collier, unpublished observation). Examination of the histology of prostate glands from moribund *Rosa26*-SB11;T2/onc low-copy mice revealed focal areas of epithelial hyperplasia in the anterior prostate (data not shown) and dorsolateral prostate (Supplemental Fig. 1A, B). Immunohistochemistry (IHC) suggested that the difference in prostatic phenotype for the two models could be explained by differences in transposase expression in the prostate gland (Supplemental Fig. 2).

The prostates of *Rosa26*-SB11;T2/onc low-copy mice were also evaluated using proliferation markers Ki67 (20) and phospho-(ser10)-histone H3 (21). In single transgenic control prostates (*Rosa26*-SB11 or T2/onc low-copy only), Ki67 positive cells were rare and typically found as single positive cells or a pair of positive cells (Supplemental Fig. 1C–D). In contrast, *Rosa26*-SB11;T2/onc low-copy double transgenic mice contained focal areas with many Ki67 positive cells (Fig. 1). A quantitative analysis of the distribution of Ki67 positive cells confirmed the increased clustering of Ki67 positive cells into focal areas of elevated proliferation in

Rosa26-SB11;T2/onc low-copy prostates relative to controls (Fig. 2A). In addition to the change in the distribution of proliferating cells, an overall increase in the number of proliferating prostatic epithelial cells was observed in *Rosa26*-SB11;T2/onc low-copy mice with both Ki67 and phospho-(ser10)-histone H3 (data not shown).

Identification of transposon insertion sites in prostatic hyperplasia

After failed initial attempts to identify transposon insertion sites present in the prostatic lesions using laser capture microscopy, the limits of the published linker-mediated PCR (LM-PCR) method (4,5) were evaluated using DNA from two mice with well characterized transposon insertions inherited through the germline (22). These mice lacked transposase expression so all somatic cells from each animal harbored identical transposon insertions. LM-PCR on serial dilutions of high quality DNA showed that the isolation of transposon-flanking sequences became unreliable in the low-ng range (Fig. 2B). A modified protocol (see Materials and Methods) allowed the reliable identification of the known transposon insertion sites from approximately 100 laser captured cells isolated from these animals (data not shown). When this protocol was used to identify the transposon insertion sites present in foci of proliferation (clusters of 3 or more phospho-ser10-histone H3 positive cells) from *Rosa26*-SB11;T2/onc low-copy prostates, complex banding patterns were observed following LM-PCR that varied from sample to sample (Fig. 2C).

In order to identify genes that can initiate proliferation/hyperplasia in the prostatic epithelium, 100 proliferating clusters of prostatic epithelial cells were laser captured from the prostates of 20 transposon-mutagenized mice on an otherwise wild type genetic background (median animal age 6 months), and 85 proliferating clusters of prostatic epithelial cells were captured from the prostates of 17 transposon mutagenized mice deficient for *Arf* (median animal age 11 weeks). The laser-captured lesions were analyzed by LM-PCR, and the LM-PCR products were sequenced to determine the transposon insertion sites. Unique genomic sequences were mapped back onto the mouse genome using the mouse genome database maintained by the Wellcome Trust Sanger Institute at www.ensembl.org. This analysis identified 77 unique insertions isolated from prostatic lesions generated by mutagenesis on a wild type genetic background and 27 unique insertions isolated from prostatic lesions generated by mutagenesis on the *Arf*-null background. Insertions were distributed across most mouse chromosomes (Fig. 2D). The two chromosomes that harbored T2/onc concatomers in the experiment (chromosomes 1 and 15) had an increased frequency of insertions that was expected due to the tendency of transposons to mobilize at higher frequency to locations linked to the donor transposon concatomer (23), a phenomenon called local hopping. The prostate insertions were evaluated using previously proposed criteria for CIS identification (24). Using these criteria, 3 CISs were found in the prostate data set. The three genes at prostate CISs in the experiment were *Rabgap1l, Pde4d*, and *Klhl13* (Supplemental Table 1). *Rabgap1l* is known to be located very close to the chromosome 1 T2/onc donor concatomer (5). Consequently, this gene may have been repeatedly mutated due to local hopping. The other two genes located at CISs were not linked to the T2/onc concatomers utilized in the experiment so mutation of these genes likely contributed to the abnormal proliferation observed in the prostatic epithelium. Insertions in *Pde4d* were observed in proliferating lesions isolated from three independent mice. However, all of the insertions were in intron 5 with the MSCV promoter in T2/onc oriented toward exon 6 of *Pde4d*. *Pde4d* encodes several alternatively spliced transcripts including short-isoform transcripts that initiate translation at an in-frame AUG codon with a strong Kozak consensus located in exon 6 (Fig. 3). Thus, the T2/onc insertions would be predicted to cause over-expression of one or more endogenous short isoforms of *Pde4d* in prostatic epithelial cells. Transposon insertions in *Klhl13* were observed in both promoter orientations.

The prostate insertion sites observed in this experiment were also compared to previously reported retroviral and transposon insertions from other cancer screens by searching the Retroviral Tagged Cancer Gene Database [RTCGD; (25)]. Both *Rabgap1l* and *Pde4d* have been previously observed as CISs in other somatic mutagenesis screens for cancer genes (5, 26) while *Klhl13* is a novel CIS. Since many oncogenes and tumor suppressor genes function in multiple tumor types, we hypothesized that the combined prostate and RTCGD data sets may identify new CISs. Using the criteria proposed by Mikkers et al. (24) for the approximately 8700 insertions in the combined data sets, five novel CISs were identified (Supplemental Table 2). Among the remaining insertion sites isolated from prostatic lesions, eleven were insertions into genes previously reported as CISs (Supplemental Table 3).

Overexpression and mRNA isoform changes for *PDE4D* in human prostate cancer

To investigate the possibility that PDE4D is involved in human prostate cancer, we collaborated with the laboratory of a board-certified surgical pathologist, Wei Huang, MD. The Huang laboratory had previously assembled a tissue microarray (TMA) of prostate tissues from patients treated at the University of Wisconsin-Madison including patients with benign prostatic hyperplasia (BPH) and patients with prostatic adenocarcinoma (17). The approach used for analyzing PDE4D protein expression on the TMA was a previously described method (18) for automated quantitative analysis (AQUA). For the AQUA approach, proteins were detected using fluorescence-based immunohistochemistry. The TMA was co-stained with the antibody against PDE4D, an epithelial cytoplasm-specific antibody cocktail (E-cadherin and anti-cytokeratin antibodies), and a nuclear stain (DAPI). The stained TMA was then imaged using a series of fluorescent filters corresponding to each stain, and the images were analyzed using previously developed algorithms (18) to determine relative expression levels of PDE4D. A parallel TMA was analyzed in which the anti-PDE4D antibody was blocked with a PDE4D peptide to confirm specificity of the PDE4D signal. A strong PDE4D-specific signal was observed for the PDE4D antibody that co-localized with the E-cadherin/cytokeratin stains in human prostatic adenocarcinomas (Figure 4A). The prostate TMA cores from patients with prostatic adenocarcinoma varied in pathological grade (as scored by surgical pathologist Wei Huang, MD) and included cores that were primarily composed of non-invasive epithelial cells (normal or PIN), cores that were primarily invasive cancer, and cores from sites of metastasis. When the AQUA data was quantified and stratified by these pathologic features, all prostate tissues from patients with adenocarcinomas had higher PDE4D expression than tissues from patients with BPH (Figure 4B). No significant differences in PDE4D expression level were observed among the different pathological grades for tissue cores from prostate cancer patients. PDE4D expression in prostate cancer was also evaluated by immunoblotting in normal primary prostatic epithelial cells and 5 common prostate cancer epithelial cell lines. PDE4D protein expression was increased in the human prostate cancer cell lines compared to normal primary prostatic epithelial cells (Supplemental Fig. 3).

To further understand the expression of *PDE4D* in human prostate cancer, pooled RNA from samples of pathologically normal prostate and prostatic adenocarcinomas were evaluated by RNA ligase-mediated 5' Rapid Amplification of cDNA Ends [RLM-5'-RACE; (27)]. The predominant RLM-5'-RACE products from normal prostate and prostate cancer RNAs were distinct (Fig. 4C), suggesting altered *PDE4D* isoform expression in human prostate cancer. Sequencing of the predominant RLM-5'-RACE product obtained from the pooled prostatic adenocarcinoma RNA identified a cDNA with a first exon that began at base pair 349 of the Genbank deposited sequence for the *PDE4D5* isoform (accession AF12073.1) and was spliced to exon 2 of *PDE4D* in a manner identical to the other *PDE4D* long isoform transcripts.

PDE4D knockdown reduces the growth rate of human prostate cancer cells and xenografts

As an initial test of the functional role of PDE4D in prostate cancer cells, PDE4D protein expression was reduced in DU145 and PC3 cells using three different shRNAs targeting sequences in *PDE4D* (Fig 5). Based on densitometry of immunoblots with an anti-PDE4D antibody, these shRNAs achieved 70–97% knockdown of PDE4D protein expression (data not shown). In all cases, the knockdown cell populations had significantly reduced *in vitro* growth rates compared to control cells with stable transfection of scrambled sequence shRNAs (Fig. 5A–C). The impact of PDE4D knockdown on cell migration was also evaluated using an *in vitro* wound healing assay, and PDE4D knockdown significantly decreased the migration rate of DU145 cells (Supplemental Fig. 4).

To further evaluate the role of PDE4D in prostate cancer cells, we used the exon 14/15 PDE4D knockdown and scrambled shRNA control DU145 cell lines in a xenograft model. PDE4D knockdown resulted in smaller xenografts compared to control tumors (Fig. 6A; Supplemental Fig. 5A). The reduction in wet weight of the PDE4D knockdown xenografts was statistically significant, but there was considerable variability in wet weight among the xenografts in each group due to the presence of large cysts lacking viable tumor cells in many of the xenografts (Supplemental Fig. 5B–D). Consequently, we also assayed tumor cell proliferation using immunostaining for the Ki67 antigen. Analysis of the Ki67 labeling index for PDE4D knockdown and control xenografts found a statistically significant 39.0% reduction ($p<0.01$, by T-Test) in the Ki67 labeling index for knockdown tumors relative to controls (Fig. 6B–D) indicating a reduced proliferation rate in response to PDE4D knockdown. We also examined apoptosis in the xenografts using a TUNEL assay. While moderate rates of apoptosis were observed in all xenografts, no significant differences were observed between the control shRNA and PDE4D knockdown tumors (data not shown) suggesting that the reduction in tumor size was primarily due to decreased proliferation in response to PDE4D knockdown.

DISCUSSION

Genetic screens in model organisms have been an important strategy for understanding the molecular genetics of several cancers. For many years, one of the most productive screening approaches has been the use of slow transforming retroviruses as insertional mutagens to tag and identify endogenous oncogenes and tumor suppressor genes in mice [reviewed in (28)]. Screens using retroviruses have investigated several tumor types including mammary tumors, hematopoietic neoplasms, and brain tumors. These screens have identified genes and genetic interactions that have proven to be directly relevant for understanding the equivalent human cancers. One of the major limitations of retroviruses as a screening tool is their cell-type specificity that defines the types of tumors they can induce. This has prevented retroviral-based screens for many of the most common tumor types in humans.

Recently, the SB transposon system has been shown to function as an insertional mutagen to discover cancer genes for hematopoietic tumors, medulloblastomas, and sarcomas in genetically modified mice (4,5). These initial proof-of-principle studies showed that mobilization of transposons engineered to have gain- and loss-of-function elements could accelerate tumor formation, and cloning transposon insertion sites identified candidate cancer genes at CISs. Transposon-based screening has great potential because mobilization of the transposon is not cell-type restricted so screens are possible in tissues not amenable to retroviral screens such as the sarcomas investigated by Collier, Carlson *et al*. However, it had previously not been determined if transposon-based screens can be used to investigate epithelial tumors that constitute the majority of human cancers. In addition, although the candidate cancer genes at the CISs observed by Dupuy *et al*. and Collier, Carlson *et al*. included genes not previously implicated in cancer, it is not yet clear whether these candidate cancer genes will prove to be relevant for understanding disease processes in humans.

The current study addresses these issues by investigating transposon-mutagenized mice for prostate cancer related phenotypes. The prostates of *Rosa26*-SB11;T2/onc low-copy mice had focal areas of epithelial hyperplasia and elevated epithelial proliferation that resembled features of prostate cancer precursor lesions. Cloning transposon insertion sites from these lesions identified candidate cancer genes at transposon CISs. We conducted our screen using both wild type and *Arf*-null genetic backgrounds. Insertions were observed at newly identified and previously known CISs on both genetic backgrounds. Based on the CISs in the Retroviral Tagged Cancer Gene Database (25), about 2.2% of all genes have been identified as CISs in one or more cancer screens. For our screen, 19% of insertions on a wild type genetic background were into CIS genes reflecting a 9-fold enrichment over what would be predicted by chance. For insertions on the *Arf*-null background, 41% of insertions were into CIS genes reflecting a 19-fold enrichment over what would be predicted by chance. These data suggest that most of the insertions into CIS genes in our screen were likely to be selected insertions that contributed to the focal prostate epithelial hyperplasia and proliferation observed in *Rosa26*-SB11;T2/onc low-copy mice. Further investigation of one of the CIS genes, *Pde4d*, showed that it is a mitogenic factor for prostatic epithelial cells that is also over-expressed in human prostate cancers. Thus, transposon-based screens in mice can discover novel genes that are directly relevant for understanding human prostate cancer.

PDE4D is a gene encoding several phosphodiesterase enzymes that cleave cAMP and are expressed in multiple tissues (29–34). *PDE4D* encodes at least nine protein isoforms that all possess the phosphodiesterase catalytic domain in the C-terminus but differ at the N-terminus. The nine isoforms are categorized into two groups: long isoforms (3,4,5,7,8,9) and short isoforms (1,2,6). In our study, we identified multiple transposon insertions into the mouse *Pde4d* gene that are predicted to cause overexpression of one or more short isoforms. A previous investigation of rats that had increased susceptibility to prostate carcinogenesis due to developmental exposure to estrogens found increased expression of *PDE4D4*, one of the long isoforms, in the prostates of susceptible rats (35). This led the authors to hypothesize that *PDE4D* overexpression had a causal role in prostate cancer susceptibility in the rat model. Our finding that PDE4D protein is overexpressed in the prostatic epithelial cells of patients with prostatic adenocarcinoma relative to patients with the benign disease BPH regardless of the histopathology of the epithelial cells in the adenocarcinoma patients (normal, PIN, invasive cancer, metastasis) suggests PDE4D overexpression in the aging human prostate may also be a permissive event that increases susceptibility to prostate cancer.

The status of PDE4D in human prostate cancer had not previously been specifically investigated, but genome-wide expression profiling studies of human prostate cancer often included probes against *PDE4D* transcripts. We reviewed *PDE4D* for expression changes in the available prostate cancer expression profiling studies using the Oncomine Database (36). The available expression profiling studies generally observed no change for *PDE4D* mRNA expression or a decrease in expression with increasing pathologic grade of prostate cancer. The potential discrepancy between our finding of an increase in PDE4D protein expression in prostate cancer patients and the decreased *PDE4D* mRNA expression observed in some expression profiling studies may reflect post-transcriptional regulation of PDE4D. Comprehensive side-by-side analyses of mRNA and protein expression for multiple *PDE4D* isoforms in the rat have found a poor correlation between mRNA and protein expression levels for multiple *PDE4D* isoforms. This has led to the hypothesis that these *PDE4D* isoforms are post-transcriptionally regulated (31). A more dramatic finding in our study was a shift in *PDE4D* isoform usage in prostate cancer that we identified in RLM-5'-RACE experiments (Fig. 4C, D). The RLM-5'-RACE protocol includes ligation of an RNA adaptor to mRNAs prior to reverse transcription in a reaction that requires the presence of a 7-methylguanosine cap at the 5'-terminus of the mRNA (27). This allows RLM-5'RACE to selectively amplify full-length cDNA 5'-ends. We infer from our data that the predominant *PDE4D* transcript in

prostatic adenocarcinomas is initiated at base pair 349 of the Genbank deposited sequence for the *PDE4D5* isoform (accession AF12073.1). Transcripts initiated at this location would not include the normal translation initiation codon for the published *PDE4D5* transcript and would presumably initiate translation at one of the in frame AUG codons present in the truncated mRNA transcript. This possibility is consistent with the size of the PDE4D protein bands observed by immunoblot in prostate cancer cell lines (Supplemental Fig. 3).

Collectively, the increased expression of PDE4D and altered isoform usage in prostate cancer cells indicate that there will be lower cAMP levels in at least some sub-cellular compartments of prostate cancer cells relative to normal prostatic epithelial cells. This correlates with previous *in vitro* studies in prostate cancer cell lines that have found that increasing levels of cAMP by stimulating adenylate cyclase with Forskolin, using cAMP analogs, or treatment with general PDE inhibitors led to growth arrest and apoptosis of prostate cancer cell lines (37–39). Our data that selectively targeting PDE4D with shRNAs also limits prostate cancer cell growth suggests that future studies with PDE4D selective inhibitors as potential anti-prostate cancer agents are warranted.

Considered more broadly, pharmacologic inhibition of the PDE4 family of enzymes induces apoptosis or inhibits growth in a variety of cancer cell types. However, the role of *PDE4D* specifically in human cancer has not been widely investigated. PDE4 family inhibition induces apoptosis in Chronic Lymphocytic Leukemia (CLL) cells (40). However, this effect may not be due to PDE4D specifically, as *PDE4D* mRNA expression was found to be lower in CLL cells than in normal peripheral blood mononuclear cells (41). Analysis of genomic copy number changes in human lung adenocarcinoma has detected homozygous deletions at the *PDE4D* locus (42). Similar studies on esophageal adenocarcinoma identified both homozygous deletions and loss of heterozygosity at the *PDE4D* locus (43), implicating *PDE4D* as a tumor suppressor gene in these two tumor types. As regulation of PDE4D activity is complex, close examination of its genomic sequence, transcriptional regulation, alternative splicing and other post-transcriptional/translational modifications will be necessary to address the contribution of *PDE4D* to tumor formation in humans. In addition, it is possible that the ability of *PDE4D* to enhance or limit tumor growth may be cell type dependent, a phenomenon that has been observed for other cancer genes such as *NOTCH1* (44).

Prostate cancer is the most common cancer in men (6) and there is considerable genetic heterogeneity among individual prostate cancers (14). Transposon-based somatic mutagenesis is a promising strategy for uncovering the genetically diverse ways that prostate tumors can evolve. This study refined the methodology for transposon-based screening to allow investigation of small lesions that resembled the initial steps of prostate cancer progression. This identified *Pde4d* as a proliferation promoting factor in the prostates of mice and humans. In addition to *Pde4d*, this study identified 18 other genes as candidate prostate cancer genes including genes at CISs in the prostate data set (Supplemental Table 1), genes at CISs for the combined prostate + RTCGD data sets (Supplemental Table 2), and prostate insertions at genes that had previously been identified as CISs (Supplemental Table 3). Among the 19 candidate prostate cancer genes identified in our study were 5 genes that have previously been investigated for their potential roles in prostate cancer including *Dpt, Notch1, Runx3, Igf1r*, and *Ghr* [representative studies: (45–49)]. The remaining 14 candidate prostate cancer genes have not previously been investigated for their potential roles in prostate cancer. Future studies are anticipated to include evaluation of these genes in human prostate cancers and additional screening for candidate cancer genes using the refined methods developed for this study.

Supplementary Material

Refer to Web version on PubMed Central for supplementary material.

ACKNOWLEDGEMENTS

REFERENCES

1. Jonkers J, Berns A. Retroviral insertional mutagenesis as a strategy to identify cancer genes. Biochim Biophys Acta 1996;1287:29–57. [PubMed: 8639705]

2. Johansson FK, Brodd J, Eklof C, et al. Identification of candidate cancer-causing genes in mouse brain tumors by retroviral tagging. Proc Natl Acad Sci U S A 2004;101:11334–11337. [PubMed: 15273287]

3. Callahan R, Smith GH. MMTV-induced mammary tumorigenesis: gene discovery, progression to malignancy and cellular pathways. Oncogene 2000;19:992–1001. [PubMed: 10713682]

4. Dupuy AJ, Akagi K, Largaespada DA, Copeland NG, Jenkins NA. Mammalian mutagenesis using a highly mobile somatic Sleeping Beauty transposon system. Nature 2005;436:221–226. [PubMed: 16015321]

5. Collier LS, Carlson CM, Ravimohan S, Dupuy AJ, Largaespada DA. Cancer gene discovery in solid tumours using transposon-based somatic mutagenesis in the mouse. Nature 2005;436:272–276. [PubMed: 16015333]

6. Jemal A, Siegel R, Ward E, et al. Cancer statistics, 2006. CA Cancer J Clin 2006;56:106–130. [PubMed: 16514137]

7. Schlesinger C, Bostwick DG, Iczkowski KA. High-grade prostatic intraepithelial neoplasia and atypical small acinar proliferation: predictive value for cancer in current practice. Am J Surg Pathol 2005;29:1201–1207. [PubMed: 16096410]

8. De Marzo AM, Marchi VL, Epstein JI, Nelson WG. Proliferative inflammatory atrophy of the prostate: implications for prostatic carcinogenesis. Am J Pathol 1999;155:1985–1992. [PubMed: 10595928]

9. Bowen C, Bubendorf L, Voeller HJ, et al. Loss of NKX3.1 expression in human prostate cancers correlates with tumor progression. Cancer Res 2000;60:6111–6115. [PubMed: 11085535]

10. Asatiani E, Huang WX, Wang A, et al. Deletion, methylation, and expression of the NKX3.1 suppressor gene in primary human prostate cancer. Cancer Res 2005;65:1164–1173. [PubMed: 15734999]

11. Tomlins SA, Mehra R, Rhodes DR, et al. TMPRSS2:ETV4 gene fusions define a third molecular subtype of prostate cancer. Cancer Res 2006;66:3396–3400. [PubMed: 16585160]

12. Tomlins SA, Rhodes DR, Perner S, et al. Recurrent fusion of TMPRSS2 and ETS transcription factor genes in prostate cancer. Science 2005;310:644–648. [PubMed: 16254181]

13. Cerveira N, Ribeiro FR, Peixoto A, et al. TMPRSS2-ERG gene fusion causing ERG overexpression precedes chromosome copy number changes in prostate carcinomas and paired HGPIN lesions. Neoplasia 2006;8:826–832. [PubMed: 17032499]

14. Abate-Shen C, Shen MM. Molecular genetics of prostate cancer. Genes Dev 2000;14:2410–2434. [PubMed: 11018010]

15. Kuslak SL, Marker PC. Fibroblast growth factor receptor signaling through MEK-ERK is required for prostate bud induction. Differentiation 2007;75:638–651. [PubMed: 17309601]

16. Largaespada DA, Collier LS. Transposon-mediated mutagenesis in somatic cells: identification of transposon-genomic DNA junctions. Methods in molecular biology (Clifton, NJ 2008;435:95–108.

17. Warren M, Twohig M, Pier T, et al. Protein expression of matriptase and its cognate inhibitor HAI-1 in human prostate cancer: a tissue microarray and automated quantitative analysis. Appl Immunohistochem Mol Morphol 2009;17:23–30. [PubMed: 18813126]

18. Camp RL, Chung GG, Rimm DL. Automated subcellular localization and quantification of protein expression in tissue microarrays. Nat Med 2002;8:1323–1327. [PubMed: 12389040]

19. Wild R, Ramakrishnan S, Sedgewick J, Griffioen AW. Quantitative assessment of angiogenesis and tumor vessel architecture by computer-assisted digital image analysis: effects of VEGF-toxin conjugate on tumor microvessel density. Microvasc Res 2000;59:368–376. [PubMed: 10792968]

20. Gallee MP, Visser-de Jong E, ten Kate FJ, Schroeder FH, Van der Kwast TH. Monoclonal antibody Ki-67 defined growth fraction in benign prostatic hyperplasia and prostatic cancer. J Urol 1989;142:1342–1346. [PubMed: 2478729]

21. Nowak SJ, Corces VG. Phosphorylation of histone H3: a balancing act between chromosome condensation and transcriptional activation. Trends Genet 2004;20:214–220. [PubMed: 15041176]

22. Geurts AM, Collier LS, Geurts JL, et al. Gene mutations and genomic rearrangements in the mouse as a result of transposon mobilization from chromosomal concatemers. PLoS Genet 2006;2:e156. [PubMed: 17009875]

23. Carlson CM, Dupuy AJ, Fritz S, Roberg-Perez KJ, Fletcher CF, Largaespada DA. Transposon mutagenesis of the mouse germline. Genetics 2003;165:243–256. [PubMed: 14504232]

24. Mikkers H, Allen J, Knipscheer P, et al. High-throughput retroviral tagging to identify components of specific signaling pathways in cancer. Nat Genet 2002;32:153–159. [PubMed: 12185366]

25. Akagi K, Suzuki T, Stephens RM, Jenkins NA, Copeland NG. RTCGD: retroviral tagged cancer gene database. Nucleic Acids Res 2004;32:D523–D527. [PubMed: 14681473]

26. Bijl J, Sauvageau M, Thompson A, Sauvageau G. High incidence of proviral integrations in the Hoxa locus in a new model of E2a-PBX1-induced B-cell leukemia. Genes Dev 2005;19:224–233. [PubMed: 15655112]

27. Liu X, Gorovsky MA. Mapping the 5' and 3' ends of Tetrahymena thermophila mRNAs using RNA ligase mediated amplification of cDNA ends (RLM-RACE). Nucleic Acids Res 1993;21:4954–4960. [PubMed: 8177745]

28. Uren AG, Kool J, Berns A, van Lohuizen M. Retroviral insertional mutagenesis: past, present and future. Oncogene 2005;24:7656–7672. [PubMed: 16299527]

29. Uckert S, Oelke M, Stief CG, Andersson KE, Jonas U, Hedlund P. Immunohistochemical distribution of cAMP-and cGMP-phosphodiesterase (PDE) isoenzymes in the human prostate. Eur Urol 2006;49:740–745. [PubMed: 16460876]

30. Uckert S, Kuthe A, Jonas U, Stief CG. Characterization and functional relevance of cyclic nucleotide phosphodiesterase isoenzymes of the human prostate. J Urol 2001;166:2484–2490. [PubMed: 11696815]

31. Richter W, Jin SL, Conti M. Splice variants of the cyclic nucleotide phosphodiesterase PDE4D are differentially expressed and regulated in rat tissue. Biochem J 2005;388:803–811. [PubMed: 15717866]

32. Bolger GB, Erdogan S, Jones RE, et al. Characterization of five different proteins produced by alternatively spliced mRNAs from the human cAMP-specific phosphodiesterase PDE4D gene. Biochem J 1997;328(Pt 2):539–548. [PubMed: 9371713]

33. Bolger G, Michaeli T, Martins T, et al. A family of human phosphodiesterases homologous to the dunce learning and memory gene product of Drosophila melanogaster are potential targets for antidepressant drugs. Mol Cell Biol 1993;13:6558–6571. [PubMed: 8413254]

34. Nemoz G, Zhang R, Sette C, Conti M. Identification of cyclic AMP-phosphodiesterase variants from the PDE4D gene expressed in human peripheral mononuclear cells. FEBS Lett 1996;384:97–102. [PubMed: 8797812]

35. Ho SM, Tang WY, Belmonte de Frausto J, Prins GS. Developmental exposure to estradiol and bisphenol A increases susceptibility to prostate carcinogenesis and epigenetically regulates phosphodiesterase type 4 variant 4. Cancer Res 2006;66:5624–5632. [PubMed: 16740699]

36. Rhodes DR, Yu J, Shanker K, et al. ONCOMINE: a cancer microarray database and integrated data-mining platform. Neoplasia 2004;6:1–6. [PubMed: 15068665]

37. Niles RM, Makarski JS, Kurtz MJ, Rutenburg AM. Inhibition of human prostatic epithelial cell replication by cAMP and selected analogs. Exp Cell Res 1976;102:95–103. [PubMed: 185073]

38. Bang YJ, Pirnia F, Fang WG, et al. Terminal neuroendocrine differentiation of human prostate carcinoma cells in response to increased intracellular cyclic AMP. Proc Natl Acad Sci U S A 1994;91:5330–5334. [PubMed: 8202489]

39. Bang YJ, Kim SJ, Danielpour D, et al. Cyclic AMP induces transforming growth factor beta 2 gene expression and growth arrest in the human androgen-independent prostate carcinoma cell line PC-3. Proc Natl Acad Sci U S A 1992;89:3556–3560. [PubMed: 1373503]

40. Kim DH, Lerner A. Type 4 cyclic adenosine monophosphate phosphodiesterase as a therapeutic target in chronic lymphocytic leukemia. Blood 1998;92:2484–2494. [PubMed: 9746789]

41. Zhang L, Murray F, Zahno A, et al. Cyclic nucleotide phosphodiesterase profiling reveals increased expression of phosphodiesterase 7B in chronic lymphocytic leukemia. Proc Natl Acad Sci U S A 2008;105:19532–19537. [PubMed: 19033455]

42. Weir BA, Woo MS, Getz G, et al. Characterizing the cancer genome in lung adenocarcinoma. Nature 2007;450:893–898. [PubMed: 17982442]

43. Nancarrow DJ, Handoko HY, Smithers BM, et al. Genome-wide copy number analysis in esophageal adenocarcinoma using high-density single-nucleotide polymorphism arrays. Cancer Res 2008;68:4163–4172. [PubMed: 18519675]

44. Dotto GP. Notch tumor suppressor function. Oncogene 2008;27:5115–5123. [PubMed: 18758480]

45. Takeuchi T, Suzuki M, Kumagai J, Kamijo T, Sakai M, Kitamura T. Extracellular matrix dermatopontin modulates prostate cell growth in vivo. J Endocrinol 2006;190:351–361. [PubMed: 16899568]

46. Hellawell GO, Turner GD, Davies DR, Poulsom R, Brewster SF, Macaulay VM. Expression of the type 1 insulin-like growth factor receptor is up-regulated in primary prostate cancer and commonly persists in metastatic disease. Cancer Res 2002;62:2942–2950. [PubMed: 12019176]

47. Fowler M, Borazanci E, McGhee L, et al. RUNX1 (AML-1) and RUNX2 (AML-3) cooperate with prostate-derived Ets factor to activate transcription from the PSA upstream regulatory region. J Cell Biochem 2006;97:1–17. [PubMed: 16237704]

48. Shou J, Ross S, Koeppen H, de Sauvage FJ, Gao WQ. Dynamics of notch expression during murine prostate development and tumorigenesis. Cancer Res 2001;61:7291–7297. [PubMed: 11585768]

49. Weiss-Messer E, Merom O, Adi A, et al. Growth hormone (GH) receptors in prostate cancer: gene expression in human tissues and cell lines and characterization, GH signaling and androgen receptor regulation in LNCaP cells. Mol Cell Endocrinol 2004;220:109–123. [PubMed: 15196705]

50. Wu X, Li Y, Crise B, Burgess SM. Transcription start regions in the human genome are favored targets for MLV integration. Science 2003;300:1749–1751. [PubMed: 12805549]
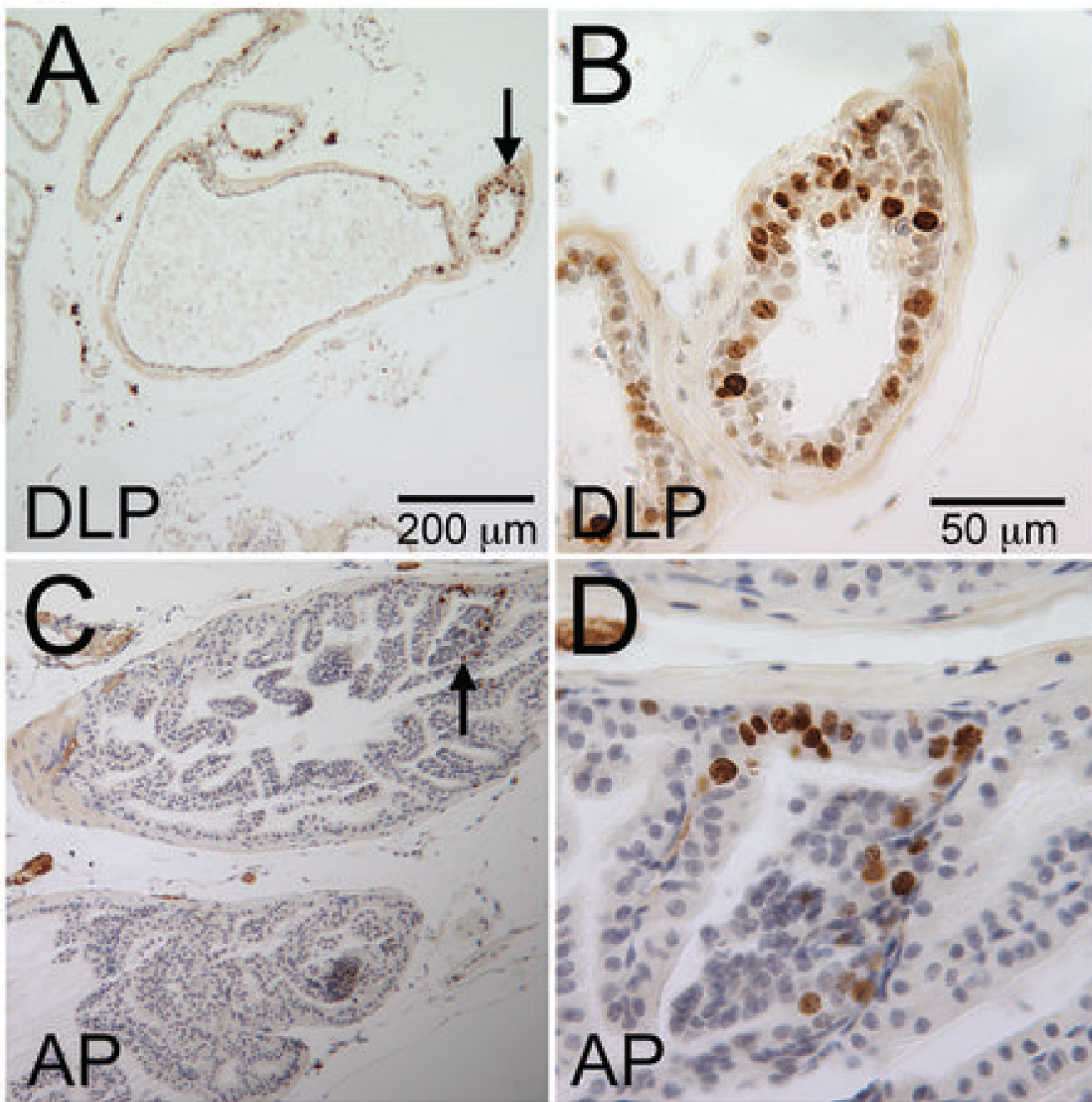
Figure 1. Focal areas of elevated proliferation in the prostates of *Rosa26*-SB11;T2/onc mice
The possibility that the focal areas of hyperplasia in *Rosa26*-SB11;T2/onc low-copy double
transgenic mice resulted from focal areas of increased proliferation was investigated by staining
Rosa26-SB11;T2/onc low-copy double transgenic mice and single transgenic littermate
(*Rosa26*-SB11 only or T2/onc low-copy only) controls with an antibody against the
proliferation-associated Ki67 antigen (20,21). Single transgenic control prostatic tissue
sections contained rare Ki67 positive cells that typically appeared as individual cells or a pair
of positive cells (see Supplemental Fig. 1). (A, B) Double transgenic *Rosa26*-SB11;T2/onc
low-copy prostatic tissue sections contained clusters of multiple Ki67 positive cells in the
dorsolateral prostate (example indicated by the arrow in A and shown at higher magnification

in B). (C, D) Similar clusters of multiple Ki67 positive cells were observed in the anterior prostate (example indicated by the arrow in C and shown at higher magnification in D). Scale bars are shown for A and C in A, and for B and D in B.
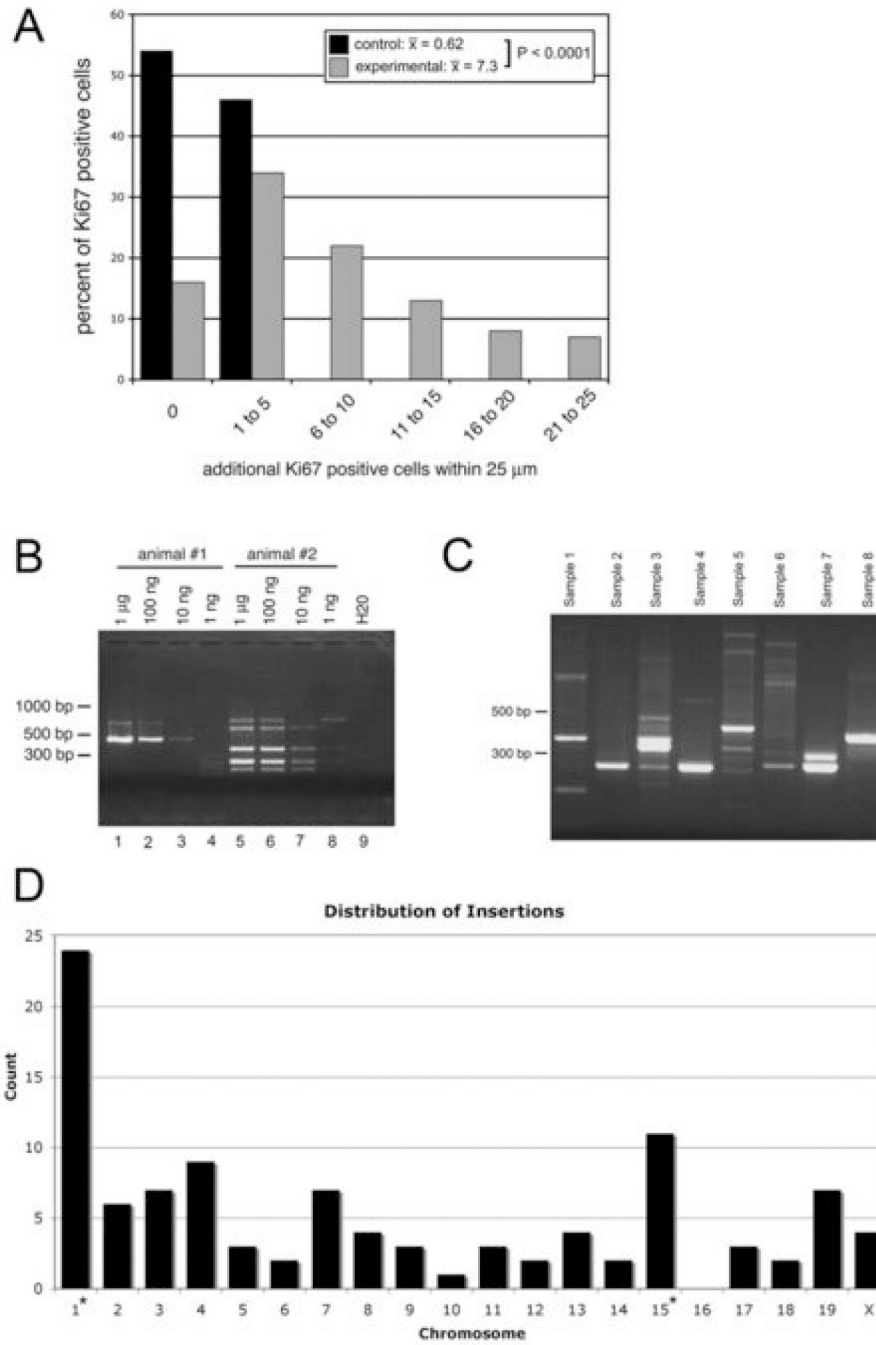
Figure 2. Analysis of proliferating prostatic lesions in *Rosa26*-SB11;T2/onc low-copy mice
To quantify the altered pattern of proliferation in the prostates of *Rosa26*-SB11;T2/onc low-copy mice, Ki67 positive cells were photographed and additional Ki67 positive cells within 25 µm were counted (n=61 for single transgenic controls, n=133 for double transgenic experimental mice). (A) Plot of the distribution of Ki67 positive cells relative to the number of additional Ki67 positive cells within 25 µm is shown. In single transgenic control prostates, there were an average of 0.62 additional Ki67 positive cells within 25 µm of a Ki67 positive cell. In *Rosa26*-SB11;T2/onc low-copy prostates, there were an average of 7.3 additional Ki67 positive cells within 25 µm of a Ki67 positive cell. The altered distribution of Ki67 positive cells for *Rosa26*-SB11;T2/onc low-copy prostates relative to single transgenic controls was

highly significant (P<0.0001 by T-test). (B) When initial attempts to isolate transposon-genomic DNA junctions from laser captured proliferating prostatic lesions failed, the limitations of published linker mediated PCR protocols for cloning transposon-genomic DNA junctions (4,5,50) were evaluated using serial dilutions of genomic DNA isolated from two mice with defined transposon insertions inherited through the germline. Animal #1 (left 4 lanes) harbored a single insertion while animal #2 (right 4 lanes) harbored 5 insertions. All insertions were reproducibly amplified from either 1µg (lanes 1 and 5) or 100ng (lanes 2 and 6) of genomic DNA, but amplification was unreliable at low-ng quantities of DNA (lanes 3, 4, 7, and 8) and failed when DNA samples were isolated from approximately 100 laser-captured prostatic cells (data not shown). (C) Modified protocols for linker-mediated PCR and immunohistochemistry were used to achieve efficient amplification of transposongenome junction fragments from laser captured cells isolated from tissue sections stained with an antibody against proliferation-associated marker phospho-(ser10)-Histone H3. When laser-captured proliferating lesions from the prostates of *Rosa26*-SB11;T2/onc low-copy double transgenic mice were analyzed by linker-mediated PCR, a variety of flanking genomic sequences were amplified and the pattern of amplified genomic fragments varied from lesion-to-lesion (samples 1–8). (D) The chromosome distribution of unique genomic insertion sites (n=104) isolated from laser-captured proliferating lesions is shown with the asterisks indicating chromosomes harboring the T2/onc transgenic concatomers used in the experiment. Approximately 34% of the insertions were linked to the donor T2/onc concatomers while the remaining insertions were distributed across 17 of the 18 other chromosomes.
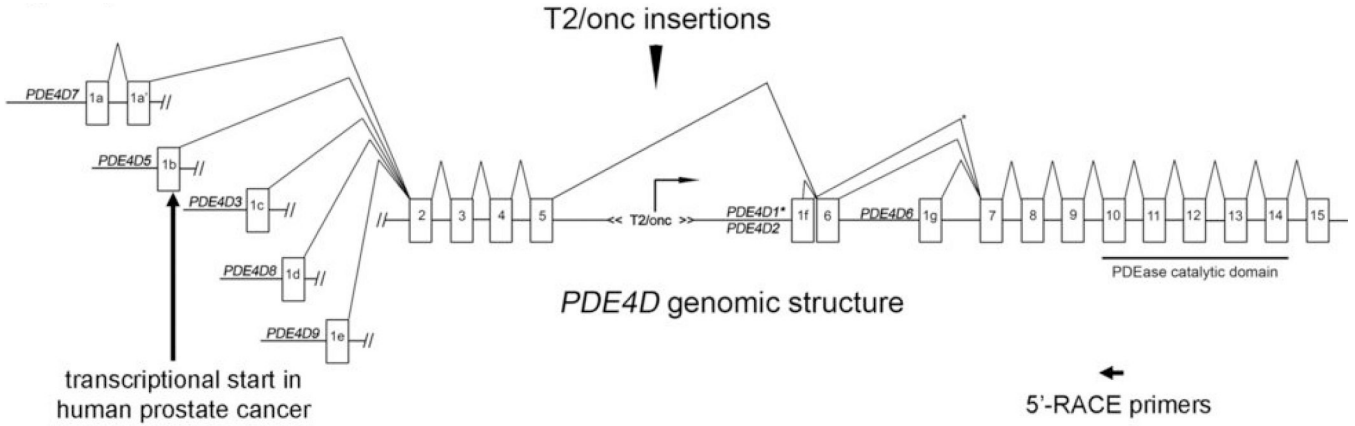
Figure 3. Transposon insertion sites in *PDE4D*
The *PDE4D* gene produces multiple protein isoforms by using alternative promoters and alternative splicing. At least 9 isoforms are made in rodents (31) and human orthologues for 8 of the 9 rodent isoforms have been reported and deposited in GenBank. The human pattern of *PDE4D* mRNA alternative splicing is similar to the rodent pattern and is depicted in the figure based on investigator-deposited GenBank transcripts (accession numbers: U50157.1, U50158.1, U50159.1, AF012073.1, AF536975.1, AF536976.1, AF536977.1, AY245867.1). There are 7 alternatively used first exons shown as 1a-1g that initiate transcription for the 8 mRNA isoforms *PDE4D1-3* and *PDE4D5-9*. All isoforms include exons 7–15 that contain coding sequences for the PDE4D catalytic domain. Long isoforms (*PDE4D 3, 5, 7, 8, 9*) also include conserved sequences from exons 2–5 that encode regulatory phosphorylation sites and a dimerization domain while short isoforms (*PDE4D 1, 2, 6*) lack these domains. The position of the T2/onc insertions observed in the prostate screen relative to alternatively used exons is also shown. Activity of the promoter in T2/onc would be predicted to over-express one or more short *PDE4D* isoforms. The location of primers used for RLM-5'-RACE experiments presented in Fig. 4 are indicated below the diagram of the PDE4D as is the transcriptional start site for PDE4D in human prostatic adenocarcinomas as determined by the experiments presented in Fig. 4.
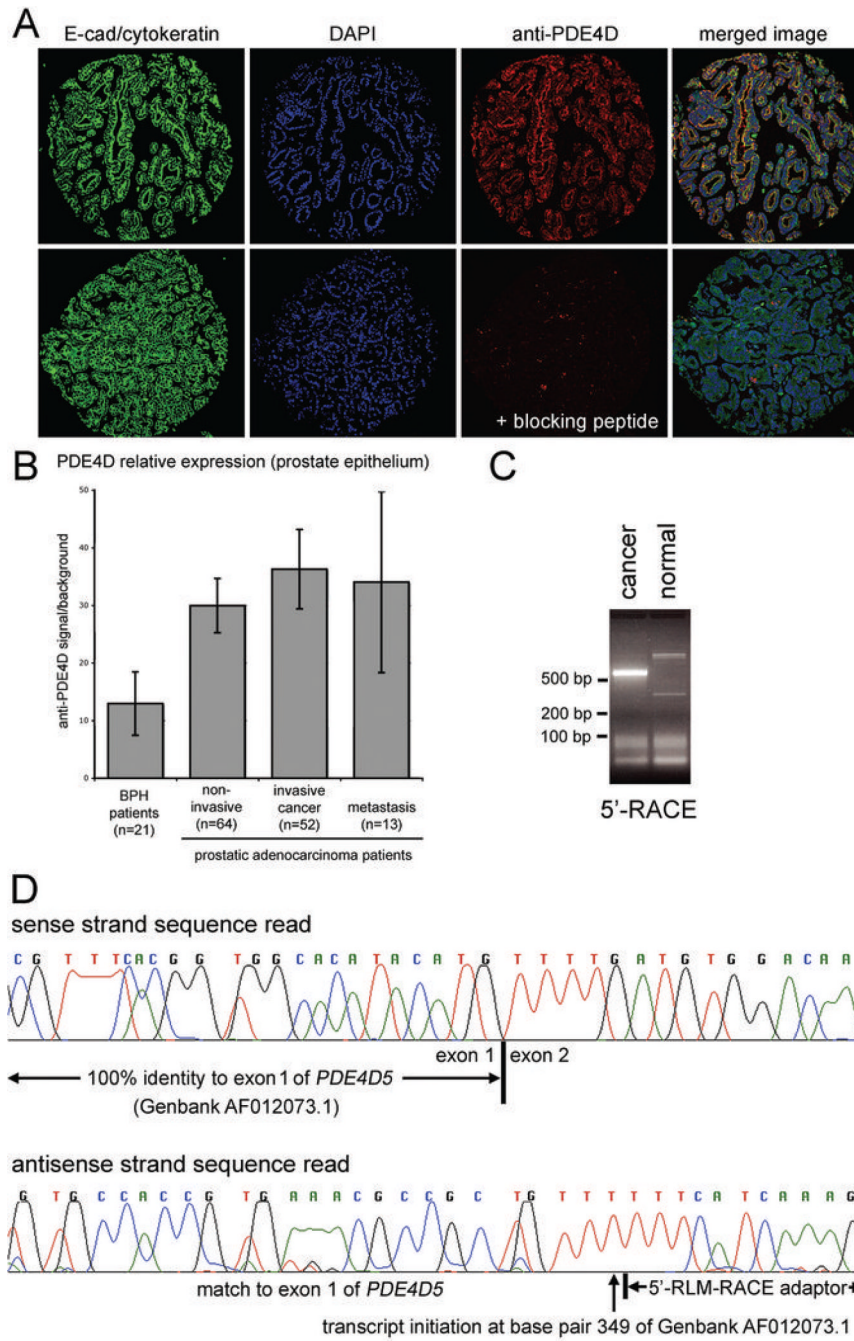
Figure 4. PDE4D is overexpressed and has altered mRNA isoform expression in human prostate cancer patient samples

(A) Fluorescent images from a prostate cancer core on a human prostate tissue microarray (TMA). The TMA was co-stained with an anti-E-cadherin/anti-cytokeratin cocktail (green channel) to identify the epithelial cell cytoplasm, DAPI (blue channel) to identify nuclei, and anti-PDE4D (red channel). PDE4D was detected in prostate cancer and co-localized with the epithelial cytoplasm-specific stain (yellow signal in top right panel). A parallel TMA was stained in the presence of a PDE4D peptide (lower row) and the anti-PDE4D signal was blocked, indicating that the anti-PDE4D signal reflected specific staining for PDE4D. (B) Graph showing the results of automated quantitative analysis (18) for PDE4D staining on the

TMA. The higher PDE4D expression level in patients with prostatic adenocarcinoma relative to patients with benign prostatic hyperplasia (BPH) was statistically significant (P<0.001 by T-test). Error bars show the 95% confidence interval. When the tissues from adenocarcinoma patients were stratified by the histopathology of the tissue core into cores that contained primarily non-invasive epithelium (normal ducts or PIN), primarily invasive cancer, or cores from sites of metastasis, the PDE4D expression level differences among the different samples from adenocarcinoma patients were not statistically significant. (C) RNA pools made from 10 prostatic adenocarcinoma samples (left lane) or 10 histologically normal prostate patient samples (right lane) were analyzed by RLM-5'-RACE using primers in exon 10 of *PDE4D* that would allow all known *PDE4D* isoforms to be amplified (location of the primers shown in Fig 3B), and the resulting pattern of amplified 5'-cDNA ends was distinct for the two pools. (D) Sequencing data are shown for the major RLM-5'-RACE product amplified from human prostatic adenocarcinoma RNA. This data showed that the first exon of the amplified transcripts began at base pair 349 of the Genbank deposited sequence for the *PDE4D5* isoform (accession AF12073.1) and was spliced to exon 2 of *PDE4D* in a manner identical to the other *PDE4D* long isoforms. The location of the inferred transcriptional start site is indicated in the diagram in Fig. 3B.
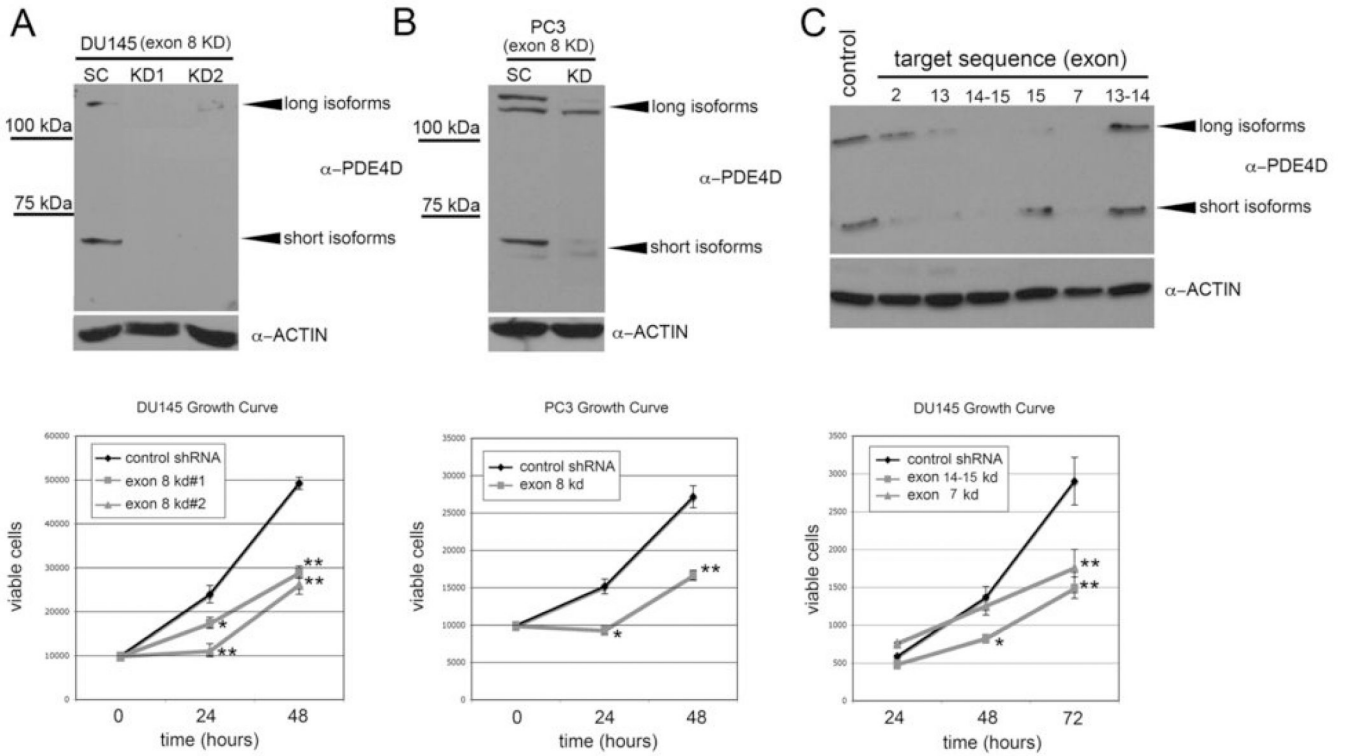
Figure 5. PDE4D shRNA knockdown reduces prostate cancer cell growth
(A) Stable transfectant variants of the DU145 prostate epithelial cell line expressing either a shRNA against a sequence in exon 8 of *PDE4D* or a scrambled control shRNA were evaluated by immunoblot for PDE4D protein expression. The control shRNA (SC) did not affect PDE4D expression while two stable transfectant pools for the *PDE4D* shRNA (KD1, KD2) had decreased expression (A, top panel). The same immunoblot was also probed with an anti-actin antibody as a loading control (A, lower blot). The growth rates of the *PDE4D* shRNA and control shRNA transfectant DU145 cells were evaluated using a trypan blue exclusion assay to quantify viable cells, and a significant decrease in growth rate was observed for cells with *PDE4D* knockdown relative to controls (A, graph). (B) The same control and *PDE4D* exon 8 shRNAs were also used to create stable transfectant variants of the PC3 prostate epithelial cell line, and PDE4D knockdown was confirmed by immunoblot (B, upper panels). The growth rates of the *PDE4D* shRNA and control shRNA transfectant PC3 cells were evaluated using a trypan blue exclusion assay to quantify viable cells, and a significant decrease in growth rate was observed for cells with *PDE4D* knockdown relative to controls (B, graph). (C) To control for off-target shRNA effects, additional shRNAs targeting other *PDE4D* exons were designed and used to create stable transfectant variants of the DU145 cell line. These variants were evaluated for PDE4D expression by immunoblot, and the most significant knockdown was observed for shRNAs directed against sequences in *PDE4D* exons 14–15 and 7 (C, upper panel). The growth rates of the exon 14–15 *PDE4D* shRNA, exon 7 *PDE4D* shRNA, and control shRNA transfectant DU145 cells were evaluated using an MTS assay to quantify viable cells, and a significant decrease in growth rate was observed for cells with *PDE4D* knockdown relative to controls (C, graph). Statistically significant differences between experimental and control data points were determined by ANOVA with least significant difference post-hoc analysis and are indicated on the graphs as follows: * P<0.05, ** P<0.001 (A and C, n=3 per data point; B, n=4 per data point).
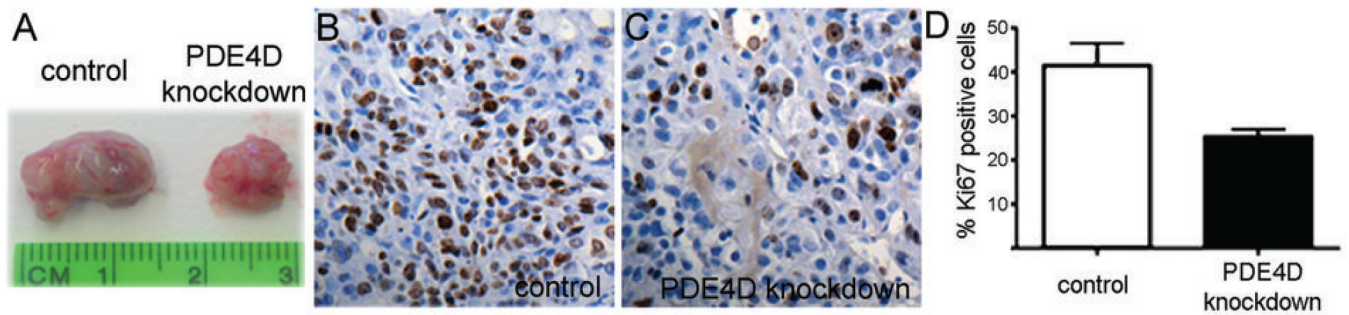
Figure 6. *PDE4D* **knockdown reduces the growth of DU145 cells** *in vivo*
Xenografts were made by injecting derivative DU145 cell lines expressing a *PDE4D*-targeting shRNA (n=7) or a scrambled sequence control shRNA (n=7) sub-cutaneously into CD-1 nu/nu male host mice (10^6 cells co-injected with matrigel). After 4 weeks of growth *in vivo*, the xenografts were harvested and photographed (examples in A). The xenograft tumors were processed for immunohistochemistry and tissue sections were stained with an antibody against proliferation-associated antigen Ki67 (brown stain in B and C). Sections were also counter stained with hematoxylin (purple stain in B and C). A high percentage of cells in the control shRNA xenografts stained positive for Ki67 (B) while a relatively lower number of cells in the *PDE4D* knockdown xenografts were Ki67 positive (C). To quantify any differences in Ki67 labeling between the two groups, 8 random 20X microscopic fields were photographed for Ki67-stained slides from each xenograft tumor (7 *PDE4D*-targeting shRNA tumors and 7 scrambled sequence control shRNA tumors) and the percentage of Ki67 positive nuclei to total nuclei was determined in the photographed areas of each tumor. The average Ki67 labeling index for control and *PDE4D* knockdown tumors is shown (D). The reduction in Ki67 labeling index observed for *PDE4D* knockdown cells was statistically significant ($p < 0.01$ by T-test).